WILEY | Hindawi

Research Article

Patchable Transparent Standalone Piezoelectric P(VDF-TrFE) Film for Radial Artery Pulse Detection

Yian Hu,[1] Shunyao Huang,[1] Yujia Gao,[1] Jaeyeon Lee,[2] Zhangsiyuan Jin,[1] Geon-Hyoung An [iD],[2,3] and Yuljae Cho [iD][1]

[1]*UM-SJTU Joint Institute, Shanghai Jiao Tong University, Shanghai 200240, China*
[2]*Department of Energy System Engineering, Gyeongsang National University, Jinju, Gyeongnam 52725, Republic of Korea*
[3]*Department of Energy Engineering, Gyeongsang National University, Jinju, Gyeongnam 52725, Republic of Korea*

Correspondence should be addressed to Geon-Hyoung An; ghan@gnu.ac.kr and Yuljae Cho; yuljae.cho@sjtu.edu.cn

Wearable or patchable biosensors have attracted tremendous attention due to their continuous health-monitoring capabilities. In particular, self-powered passive biosensors based on a piezoelectric nanogenerator (PENG) have demonstrated measurements of physiological signals from which cardiovascular information can be analyzed such as heart rate and blood pressure. However, challenges still remain with regard to both material and device aspects. For the effective and accurate measurement of extremely weak physiological signals, various methods have been introduced, including employment of inorganic lead-based piezoelectric materials and design of a complex material or device structure. In spite of their effectiveness in enhancing the piezoelectric output response, the introduced methods brought concomitant issues, such as toxicity and complexity. We present unique methods to produce a transparent standalone piezoelectric polymer film which can be directly transferred to any surface such as the human skin. Through a room temperature solvent vapor annealing process, we further enhance the crystallinity and a portion of the ferroelectric β-phase of the transparent standalone polymer film, resulting in an improved piezoelectric output response. Based on these two new methods introduced, we demonstrate a simple sandwich-structured, transparent, and patchable biosensor based on PENG for radial artery detection with significantly reduced complex manufacturing processes, providing great practical value.

1. Introduction

Population aging and health have become one of the important agenda in policy-making worldwide due to the increased demand for medical care and social welfare [1]. In particular, aged people with chronic or cardiovascular diseases without carers or in remote areas have limited access to appropriate medical resources, which severely risks their lives and leads to fatal results. Attributed to machine-learning technology, it has been forecasted that the medical care system will be fundamentally reformed in a way wherein wearable/patchable medical devices transmit physiological signals and receive feedback through the real-time health monitoring [2–4]. A question arises on how to implement a continuous health-monitoring technique without direct access to medical resources, such as cuff-based blood pressure, electrocardiography, and magnetic resonance imaging, which are not suitable for use in individuals' daily lives.

To pursue comfortable and continuous real-time health monitoring for prompt discovery of anomalies, self-powered passive flexible wearable/patchable piezoelectric or triboelectric nanogenerators (PENGs or TENGs in short, respectively) have received great attention for their biosensor applications in recent decades [5–14]. In spite of their great promise to sense physiological signals, challenges of PENGs and TENGs for the biosensor applications have also been identified [15–17]. For example, due to the nature of weak physiological signals, efforts have been made to enhance piezoelectric output response by employing lead zirconate titanate (PZT), which has a high piezoelectric constant of over 500 pC/N but includes toxic substances, or a complex

material or device configuration with composites and/or layered structures [18–22]. TENGs have provided potential solutions for the challenges in the PENG-based biosensors, attributed to their high output characteristics [23–25]. However, a structural requirement of TENGs adds further complexity to a device design and potentially compromises long-term stability of TENG-based biosensors.

Based on the viewpoints of nontoxicity and long-term stability, piezoelectric poly(vinylidene fluoride-co-trifluoroethylene), in short P(VDF-TrFE), is one of the ideal candidates for biosensor applications because it is biosafe and chemically as well as mechanically stable [26–28]. In spite of its various advantages, employment of P(VDF-TrFE) has been limited because its piezoelectric output response is relatively lower than that of its inorganic counterparts such as PZT. Fiber/textile based on P(VDF-TrFE) or its composites has been introduced, but production of fiber/textile is time and resource consuming with further requirement for complex manufacturing processes and special equipment [29–32]. Despite a continuous high demand for the piezoelectric biosensors, it has still been challenging to realize the piezoelectric biosensors based on biosafe materials without involving the complex structures.

Here, we present a unique method to produce a standalone P(VDF-TrFE) film which can achieve a piezoelectric biosensor with extremely thin thickness. This enables close contact between the active piezoelectric material and the skin. The enhanced piezoelectric output response is realized through a room temperature solvent vapor annealing (SA) method which is highly effective to enhance electrostatic interactions between the vaporized solvent molecules and P(VDF-TrFE) chains, resulting in the formation of a higher portion of the ferroelectric β-phase. In addition, the SA method turns the opaque greyish color of the P(VDF-TrFE) film into a transparent one, adding practical and aesthetic values to wearable/patchable biomedical applications. Based on the enhanced piezoelectric output and the nature of the standalone characteristic, it is possible to attain clear and precise physiological signals, enabling the further analysis of the signals for prompt detection of anomalies. On the contrary, biosensors based on a nonstandalone piezoelectric film used as a reference are only able to provide heart rate due to its nondirect contact between the human skin and the device, which suggests the importance of development of the standalone P(VDF-TrFE) film with enhanced piezoelectric output response. Furthermore, a facile and cost-effective manufacturing process provides a paradigm shift towards the piezoelectric biosensors that can be regularly changed on a daily/weekly basis for maintenance, different from conventional sensors that are embedded in other electronic systems with limited accessibility.

2. Experimental

P(VDF-TrFE) with 25 mol% of TrFE powders (Piezotech FC25) were purchased from Piezotech, Arkema. To dissolve the P(VDF-TrFE) powders, three different solvents, MEK, DMF, and DMSO, were purchased from Sinopharm Chemical Reagent (MEK) and Aladdin (DMF and DMSO). Transparent adhesive electrodes were purchased from 3M. Ammonium persulfate was purchased from Macklin. All the materials were used as received without any modifications.

2.1. Material Characterization. XRD (D8 ADVANCE DAVINCI, Bruker) was measured to characterize a phase of P(VDF-TrFE) film in the range of $2\theta = 15 \sim 25°$. Transparency of P(VDF-TrFE) films in the visible range of 400~800 nm was characterized by UV-Vis (Lambda 950, PerkinElmer). DSC (DSC 2500, TA Instruments) characterizations were carried out in a sealed sample pan at a heating rate of $10°C\,min^{-1}$ over a temperature range of 20–200°C. FTIR (Nicolet 6700, Thermo Fisher) was employed to characterize proportions of the α- and β-phases in the range of 700–1500 cm^{-1}. The PFM (MFP-3D, Oxford Instruments) measurements were performed under an applied ac voltage with the amplitude $V_{ac} = 10$. The surface potential of P(VDF-TrFE) films on glass substrates was measured using a noncontacting electrostatic voltmeter (Trek 542A, Advanced Energy).

2.2. Device Simulation. The structural mechanics module of COMSOL Multiphysics was used to simulate the piezoelectric output voltage under external pressure applied. The parameters of P(VDF-TrFE) were from our previous report [53, 54]. Pressure ranging from 9336 N/m^2 to 18664 N/m^2, corresponding to 0.0952 kg/cm^2 or 70 mmHg and 0.1903 kg/cm^2 or 140 mmHg, was applied to the model.

2.3. Device Fabrication. To fabricate devices, Cu foil was temporarily taped on a PET substrate (3M transparency film). Then, 15 wt% of P(VDF-TrFE) solution prepared in a vial was spin-coated on the Cu foil/PET substrate. For all solvents, we employed two stages of the spin-coating method, 500 rpm for 5 seconds and subsequently 3000 rpm for 30 seconds. Due to the high boiling points of DMF and DMSO, the P(VDF-TrFE) films were in a semisolid state after the spin-coating, and thus, they were spin-dried at 3000 rpm for 60 seconds one more time. The temporary PET substrates were all removed, and annealing processes were performed. Thermal annealing was performed at 130°C for 2 hours, whereas solvent vapor annealing was performed at room temperature for 40–60 minutes. The P(VDF-TrFE) films treated by solvent vapor annealing were dried at 60°C for 2 hours to completely remove residual solvents. After the annealing process, the Cu foil was etched by 0.2 M ammonium persulfate solution in DI water, leaving a free-standing P(VDF-TrFE) film. The free-standing P(VDF-TrFE) films were transferred to DI water to rinse the residue of the ammonium persulfate. After the cleaning, the free-standing P(VDF-TrFE) films were transferred to a temporary PET frame with a square-shaped hole in the middle to assemble adhesive electrodes. Finally, the temporary PET frames were cut to be removed.

2.4. Device Characterization. Piezoelectric output responses were characterized by applying mechanical pressures at various input frequencies using a linear motor (H2W Technologies). Radial artery pulses from three participants were measured by an oscilloscope (Keysight MSOX3034T)
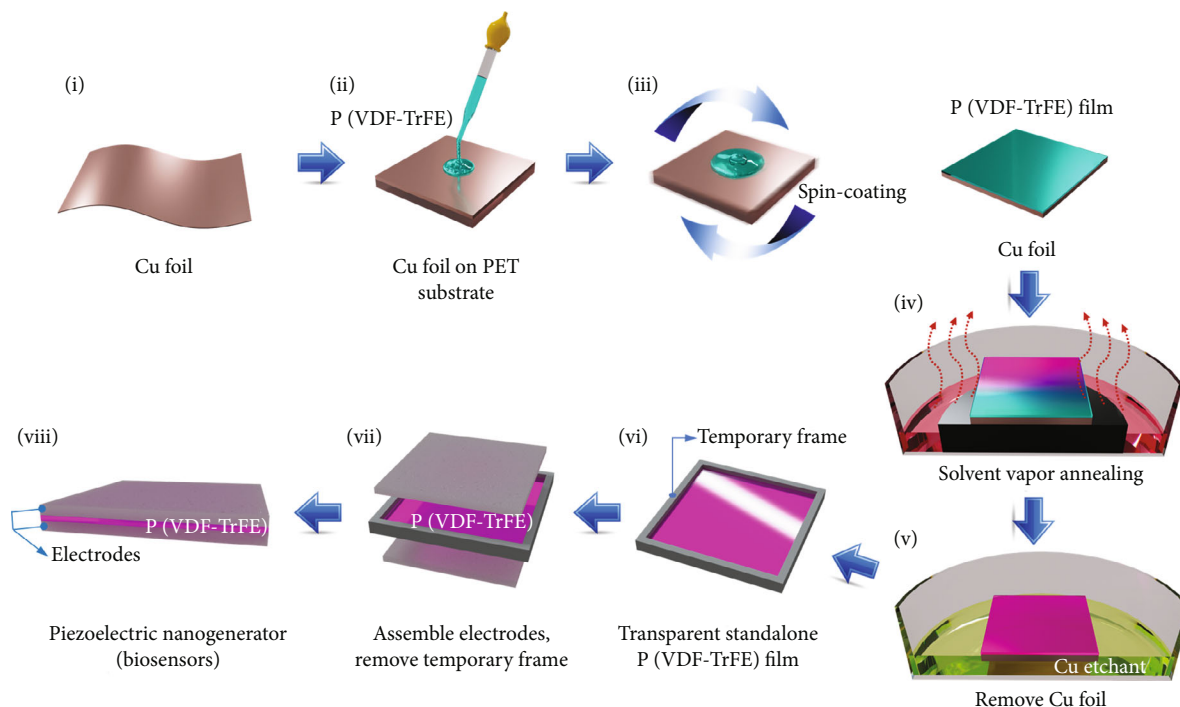
Figure 1: Schematic illustration of a preparation method of a transparent standalone P(VDF-TrFE) film and a device fabrication process.

connected with a low noise voltage amplifier (Stanford Research Systems SR560). All of the radial artery pulses were measured under a normal body condition, e.g., without illness and any exercises before the measurement.

3. Results and Discussion

Figure 1 illustrates the process to prepare a transparent standalone piezoelectric P(VDF-TrFE) film and to fabricate a patchable biosensor based on PENG for radial artery detection. (i) Cu foil with a thickness of 0.01 mm was cut into the desired size of devices ranging from mm to cm scales. (ii and iii) Then, a temporary frame to support the Cu foil was added, and a P(VDF-TrFE) solution in methyl ethyl ketone (MEK, also known as 2-butanone) was spin-coated onto the foil. (iv) The as-coated P(VDF-TrFE) film was treated by either solvent vapor annealing (SA) using MEK or the thermal annealing (TA) method to crystalize the as-coated P(VDF-TrFE) films into a ferroelectric β-phase. The SA treatment was performed for an hour, which was followed by two hours of drying at 60°C in a convection oven. The TA treatment was performed for two hours at 130°C in a convection oven. (v) The crystallized P(VDF-TrFE) film on the Cu foil was placed on a 0.2 M ammonium persulfate solution in DI to etch the Cu foil. (vi) After the removal of the Cu foil followed by the cleaning processes in DI water, the transparent standalone P(VDF-TrFE) film was attained. The standalone polymer film was transferred onto a temporary frame with a square-shaped hole in the middle by a wet transfer method which is widely used for two-dimensional material transfer, such as graphene with large sizes [33]. (vii and viii) Adhesive electrodes

were assembled to the top and bottom sides of the P(VDF-TrFE) film, and finally, four edges of the temporary frame were cut for removal, resulting in the PENG for the biosensor based on the transparent standalone P(VDF-TrFE) film.

In order to generate a high piezoelectric output for body pulse detection, a formation of a higher portion of a ferroelectric β-phase over the P(VDF-TrFE) film is an essential requirement. Mechanisms of the phase formation of P(VDF-TrFE) are correlated with various factors, including dipole moments of solvents, evaporation speed of solvents, external strain/stress applied, and so on [34, 35]. First, a solvent with a high dipole moment is preferred to induce an electrostatic interaction between dipoles of the solvent and P(VDF-TrFE) chains. When P(VDF-TrFE) is dissolved in a solvent with a high dipole moment, higher electrostatic interaction is induced, leading to the formation of the all-trans conformation, or the β-phase. Second, the evaporation speed of a solvent during the crystallization process is another factor affecting the formation of the ferroelectric β-phase. Because the β-phase has a higher potential energy than that of γ- and α-phases, the β-phase can easily transform into the intermediate γ- and stable α-phases with a lower potential energy during the crystallization process. Fast evaporation of solvents, for example, by a conventional postthermal annealing process, limits the high portion of the β-phase formation due to the reduced electrostatic interaction between the dipoles of the solvent and polymer chains before the crystallization. Therefore, it is speculated that a room- or low-temperature annealing method is preferred to effectively extend the electrostatic interaction (Figure 2(a)). In this regard, the room temperature SA method is one of the promising methods to enhance the β-
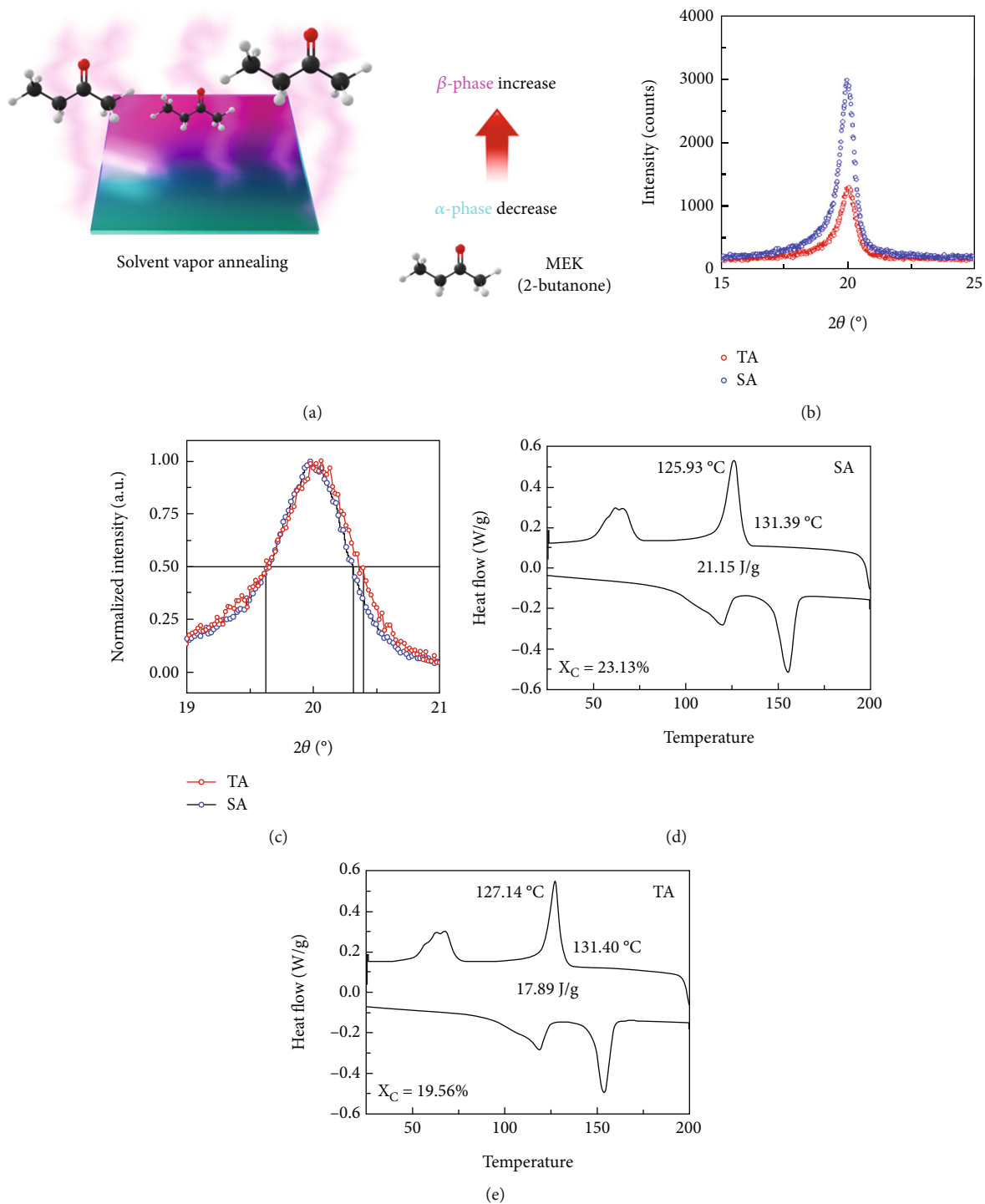
(a)

(b)

(c)

(d)

(e)

FIGURE 2: (a) Schematic illustration describing the effect of the SA method on the β-phase formation. (b) Comparison of XRD peaks of TA-TrFE in a red dotted line and SA-TrFE in a blue dotted line. (c) An enlarged image of XRD peaks in the range of $2\theta = 19 - 21°$ to determine HWHM. (d, e) DSC analysis of SA-TrFE and TA-TrFE, respectively.

phase formation as the slow-downed crystallization process enables the polymer chains to interact with the dipoles of the vapored solvent molecules for a longer period of time.

Based on these theoretical viewpoints, we employed MEK with the dipole moment of 2.76D (at 25°C) as the solvent to dissolve P(VDF-TrFE) powders and applied the SA method at room temperature [36, 37]. The vapor of the sol-

vent for the SA method effectively suppresses fast evaporation of the solvent in the P(VDF-TrFE) film, resulting in a high portion of the β-phase over the P(VDF-TrFE) film, seen from reduced FWHM from 0.77 to 0.69°, an increased percentage crystallinity (X_C) from 19.56 to 23.13%, and an increased portion of the β-phase from 82.51 to 84.35% by FTIR as shown in Figures 2(b)–2(e) and Figure S1 [34, 38].
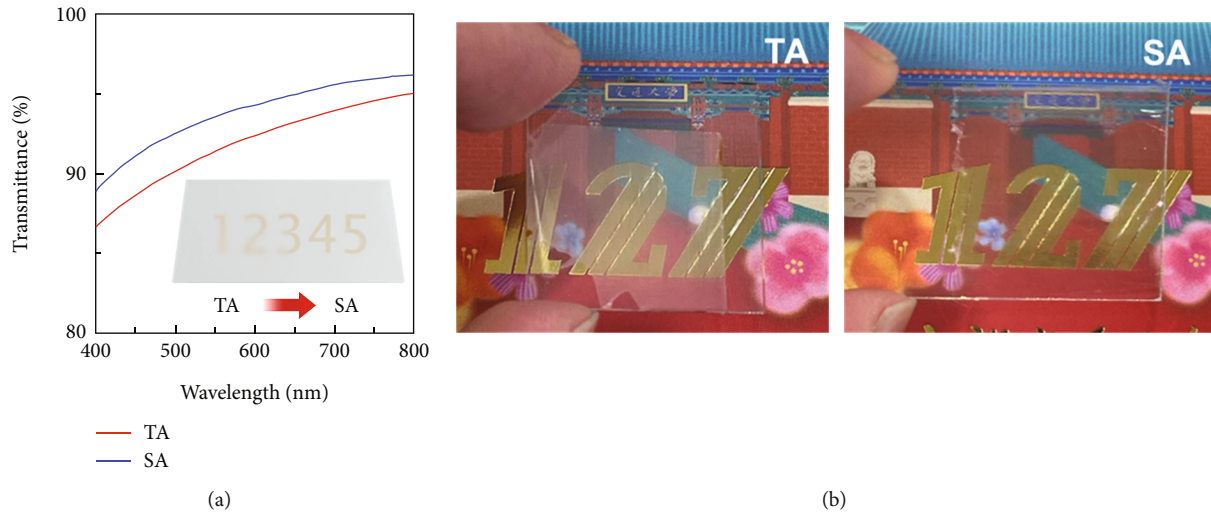
FIGURE 3: (a) Comparison of transmittance of TA-TrFE in a red solid line and SA-TrFE in a blue solid line. (b) Photographic images of TA-TrFE and SA-TrFE, denoted as TA and SA, respectively.

First, the phase formation of P(VDF-TrFE) films was analyzed via X-ray diffraction (XRD) measurement. As shown in Figure 2(b), both P(VDF-TrFE) films treated by the SA and TA methods (hereafter, SA-TrFE and TA-TrFE, respectively) showed the peak at near 20°, indicating that both annealing methods were able to form a ferroelectric β-phase [39, 40]. Taking a closer look at the XRD peaks, it is observed that the SA-TrFE film exhibited peak shift from 20.05 to 19.98°. Peak shifting to a lower value is related to the slight increase in interchain spacing, caused by gauche defects induced in the ferroelectric β-phase during the paraelectric-ferroelectric transition after cooling down from annealing, indicating that the SA-TrFE film contains a higher portion of the β-phase than the TA-TrFE film [41, 42].

In addition, the SA-TrFE film showed a narrower FWHM of 0.69° where the FHWM of the TA-TrFE was 0.77° as shown in Figure 2(c). Given that the thickness of both films was around 4 μm, measured by Dektak (Figure S2), a higher peak intensity and narrower FHWM suggest the high crystallinity of the P(VDF-TrFE) films and consequently higher portion of the β-phase formation in the SA-TrFE film [38].

Differential scanning calorimetry (DSC) was performed to extract X_C of the P(VDF-TrFE) film, which can be calculated by the following equation.

$$X_C = \left(\frac{\Delta H_m}{\Delta H_m^0}\right) \times 100\%, \tag{1}$$

where ΔH_m is the melting enthalpy of the P(VDF-TrFE) attained by DSC measurement and ΔH_m^0 is the melting enthalpy value of a 100% crystalline P(VDF-TrFE) with the value of 91.45 mJ/mg [43]. The calculated values of ΔH_m in equation (1) were 21.15 and 17.89 mJ/mg (Figures 2(d) and 2(e)), corresponding to X_C of 23.13 and 19.56% for SA-TrFE and TA-TrFE, respectively. The XRD and DSC analyses prove that the SA treatment effectively formed the

P(VDF-TrFE) film with a high portion of the β-phase and a high crystallinity of 23.13%, well consistent with the conjectures based on the theories.

Fourier transform infrared (FTIR) measurement was conducted to further confirm the proportion of the β-phase in the SA- and TA-TrFE films. As shown in Figure S1, it was observed that the peaks corresponding to the ferroelectric β-phase in the SA-TrFE film exhibited increased intensity at 840, 880, 1076, 1166, and 1398 cm^{-1}. At the same time, the wider shoulder peaks at 773 and 981 cm^{-1} which are attributed to the paraelectric α-phase were suppressed in the SA-TrFE film [44–46]. In order to quantitatively compare the proportion of the ferroelectric β-phase in SA-TrFE and TA-TrFE films, we used the equation $f_\beta = I_\beta/(1.26 \times I_\alpha + I_\beta)$, where I_α and I_β are the intensity of peaks at 763 cm^{-1} and at 840 cm^{-1}, respectively [44–46]. It was found that the proportion of the β-phase increased from 82.51 in the TA-TrFE film to 84.35% in the SA-TrFE film where $\Delta = 1.84\%$, which is well consistent with the XRD and DSC analyses.

Another merit of the SA method is its unique ability to turn the opaque greyish color P(VDF-TrFE) film into a highly transparent one, providing practical and aesthetic values for real-life applications. Transmittance measurement via ultraviolet-visible (UV-Vis) spectroscopy shows high transmittance (88.92~96.16%) of the SA-TrFE film in the range of visible light compared to the TA-TrFE film (86.69~95.05%) which is opaque and has a greyish color in Figure 3(a) where the inset illustrates this phenomenon. Digital images of SA-TrFE and TA-TrFE further visualize the clear difference of the films as shown in Figure 3(b). Attributed to the high transparency of the SA-TrFE film, the transmittance of the whole device is up to 63% where the transmittance of the transparent electrode was found to be around 83-84% in the visible range as shown in Figure S3(a)-(c).

The results from XRD and DSC analyses suggest that the SA-TrFE film will show higher piezoelectric output response
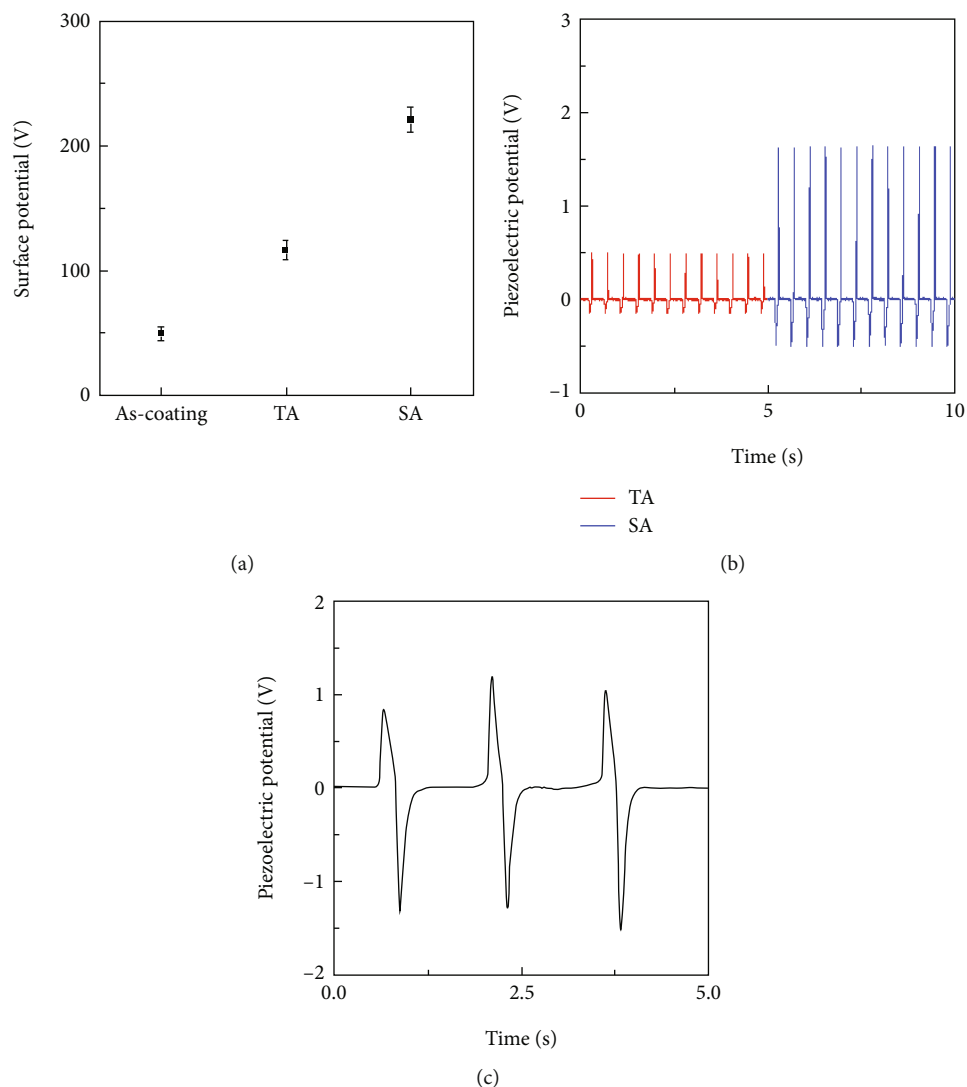
(a)

(b)

(c)

FIGURE 4: (a) Surface potential of as-coated, thermally annealed, and solvent-annealed P(VDF-TrFE) films. (b) Output potentials of fabricated PENGs with different annealing conditions. (c) Piezoelectric output response of the fabricated RAPS based on the transparent standalone P(VDF-TrFE) film.

than the TA-TrFE film, resulting from the higher portion of the ferroelectric β-phase. To confirm our conjecture, we measured a surface potential under equilibrium and the piezoelectric potential under external stimuli of TA-TrFE and SA-TrFE. As shown in Figure 4(a) and Figure S4, surface potential, measured by an electrostatic voltmeter, revealed that SA-TrFE indeed induced a higher surface potential from 116.51 to 221.17 V, which is consistent with results from XRD and DSC. As the surface potential may naturally include contributions from triboelectric charges/ potentials, to further verify our claim, we measured the piezoelectric potential of two P(VDF-TrFE) films by fabricating PENG with the structure of PET/ITO/P(VDF-TrFE)/ITO/PET without air gap between the P(VDF-TrFE) film and the top electrode. As shown in Figure 4(b), the piezoelectric output potential from SA-TrFE PENG was two to three times higher than that from TA-TrFE PENG, further proving that higher surface potential and

piezoelectric output potential are attributed to the formation of the higher portion of the β-phase and crystallinity by the SA method. The impedance of the PENG was calculated based on Ohm's law (Figure S5) and was found to be 9.5 MΩ, which is well consistent with PVDF-based energy generators with similar structure [36, 37]. Finally, our notion was further confirmed by conducting PFM measurement (Oxford Instrument, MFP-3D). Under an applied ac voltage with the amplitude $V_{ac} = 10$ V, PFM amplitude and phase were attained, and it was found that d_{33} of the SA-TrFE and TA-TrFE films is 25.46 and 22.55 pm/V, respectively, as shown in Figure S6. This further proves that a higher portion of the β-phase led to the improvement of the piezoelectric response in the SA-TrFE film.

A radial artery pulse sensor (RAPS) based on PENG was fabricated by following the process described in Figure 1. In order to confirm the piezoelectric response of the RAPS, horizontal strain at the frequency of 1 Hz was applied to
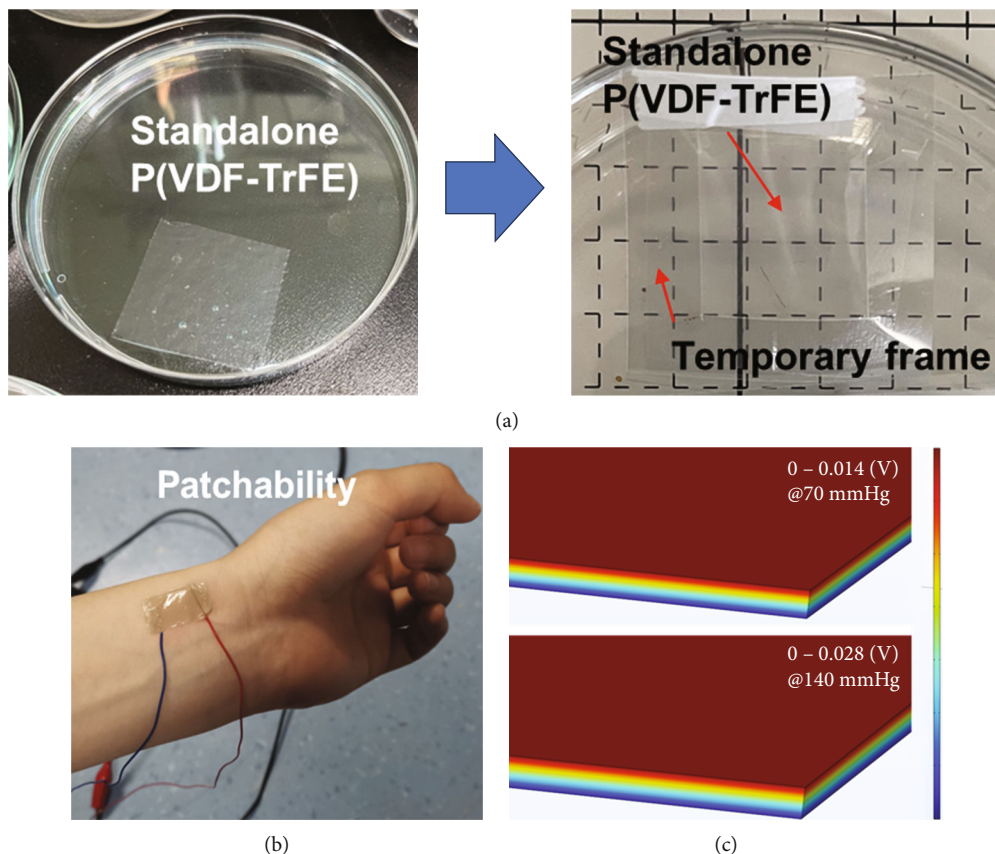
(a)

(b)

(c)

FIGURE 5: (a) Photographic images of the transparent standalone P(VDF-TrFE) films before and after the transfer on a temporary frame. (b) Photographic images of the RAPS patched to the wrist. (c) Simulated piezoelectric output potential with the input blood pressure of 70–140 mmHg.

the device. Figure 4(c) shows clear piezoelectric output responses with approximately 2 V of the peak-to-peak voltage. The frequency response of RAPS was characterized by using a linear motor with applied vertical input force of 31.2 N or 3.16 kgf to the devices under relatively low (3–40 Hz) as well as high (60–150 Hz) input frequencies as shown in Figures S7 and S8. The clear piezoelectric output response shown in Figure 4(c) and Figures S7 and S8 demonstrates that our new method is a promising way to produce the standalone piezoelectric film with higher piezoelectric output response under low to high frequency ranges.

Another benefit of our new method from a device perspective is that the production and handling of the standalone P(VDF-TrFE) films are relatively simple compared to other methods proposed previously for artery pulse detections as shown in Figures 5(a) and 5(b) [18–25]. This significantly reduces resources consumed to fabricate devices; meanwhile, the device exhibits high output signals with high accuracy, proving the effectiveness and importance of the methods developed. Attributed to these merits, the fabricated RAPS has the simple sandwiched structure readily patchable to any surfaces. Figure 5(b) illustrates the transparent RAPS based on PENG with the size of 1.5 by 1.5 cm² directly patched to the wrists of the volunteer.

Prior to the measurement of the RAPS, simulation work based on COMSOL Multiphysics was performed to predict piezoelectric output responses of the P(VDF-TrFE) film under the extremely low pressure applied by the radial artery. For example, the blood pressure of a healthy adult is generally in the range of 70–140 mmHg, which corresponds to 0.0952 kg/cm² (or 9336 N/m²)–0.1903 kg/cm² (or 18664 N/m²). The size of the P(VDF-TrFE) film used for the simulation was in the range of 10–50 mm by 10–50 mm for the width and length, respectively, and 4 μm for the thickness, which is the actual size of the RAPS. As shown in Figure 5(c), a simulated result showed piezoelectric output voltages of 14 and 28 mV at the blood pressures of 70 mmHg and 140 mmHg, respectively. This result suggests that, theoretically, the piezoelectric response of the P(VDF-TrFE) film has a high sensitivity to detect subtle blood pressures from radial artery pulses, if the material and device are properly engineered.

To further prove the effectiveness and importance of the methods developed, we compared two biosensors based on two different PENG structures: one (reference) prepared by a conventional method on a flexible substrate to ensure wearability and the other prepared by the standalone P(VDF-TrFE) film without any substrate. As shown in Figures 6(a) and 6(b), both biosensors successfully converted radial artery pulses into electric signals, providing one of the important physiological information: heart rate. In spite of the high flexibility of the reference biosensor, it is revealed
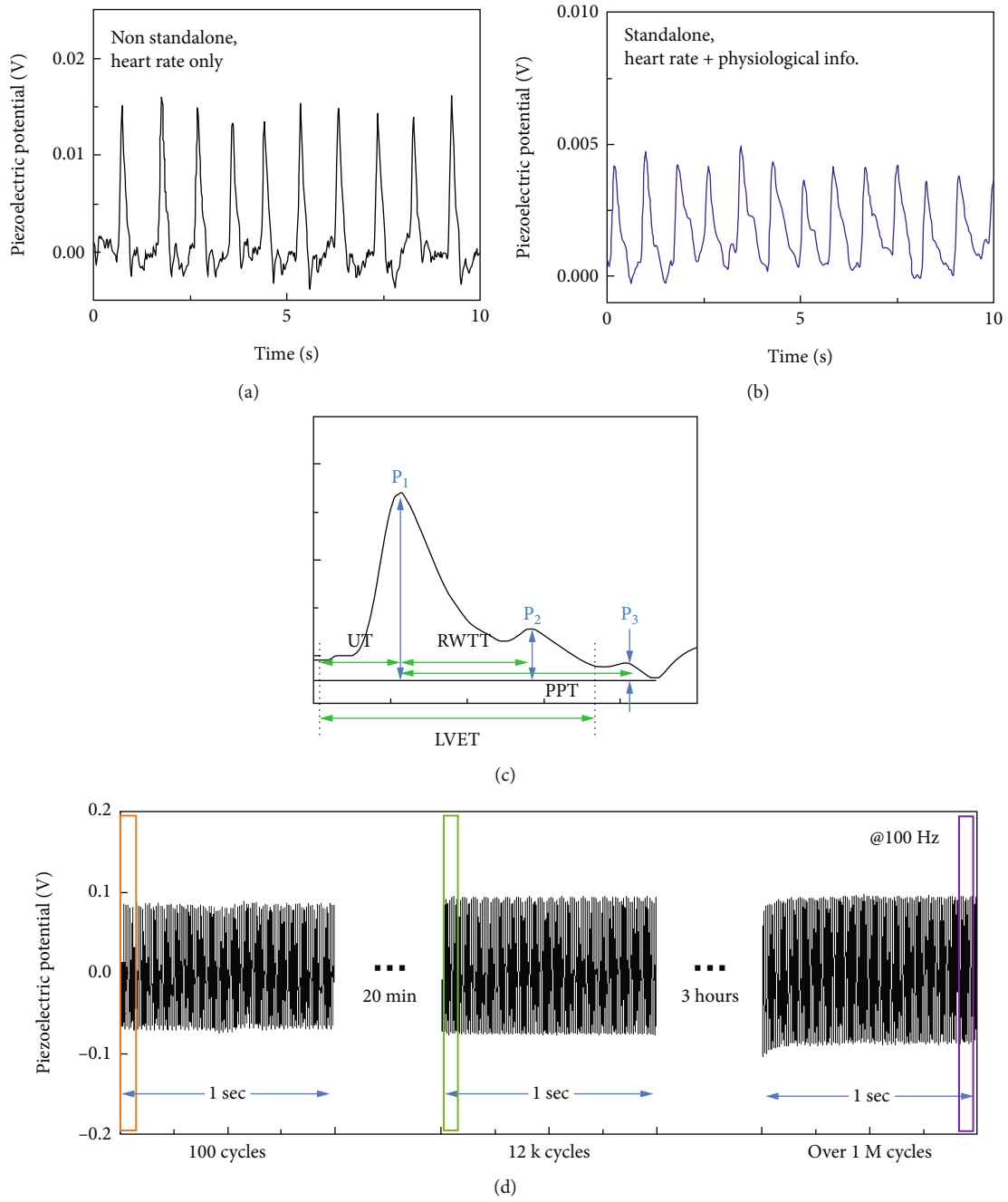
(a)

(b)
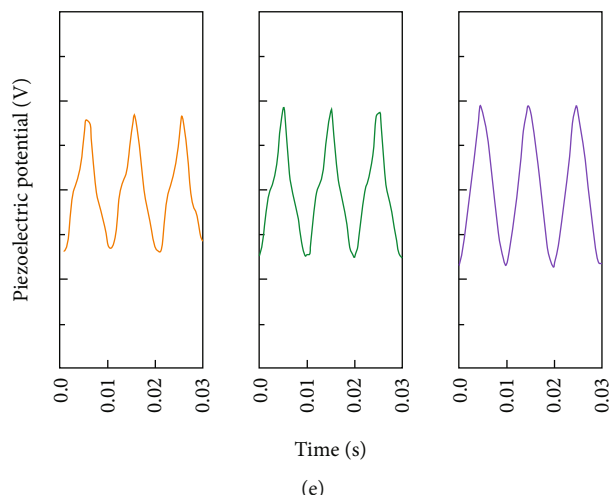

(c)

(d)

FIGURE 6: Continued.

FIGURE 6: (a) Output response of the biosensor based on the nonstandalone P(VDF-TrFE) film. (b, c) Output response and enlarged output response of RAPS generated by the radial artery pulse waves. (d) Long-term stability of RAPS excited at 100 Hz. (e) Enlarged voltage-time curves at the beginning, intermediate, and terminal stages of the stability test.

that still the existence of an additional layer in the device structure limited the accurate measurement and extraction of further physiological information through the analysis of the signals (Figure 6(a)). On the other hand, the RAPS not only revealed the heart rate of the volunteer which was 72–78 heart beats per minute (BPM) but also provided further physiological information required for the detailed analysis for a more accurate diagnosis as shown in Figures 6(b) and 6(c) and Figures S9 and S10. To be specific, a typical piezoelectric output signal of the arterial pulse includes three gradually weakening peaks, consistent with the pattern of blood pressure changes over time [47–49]. Another common behavior is that a strong reverse peak could be observed after the first positive peak point from time to time due to high blood pressure [50, 51]. As shown in Figure 6(c), the pulse waveform is composed of three peaks: (i) percussion (P) is the first systolic peak P_1 caused by the left ventricle ejection; (ii) tidal (T) is followed by the first peak and is known as the second systolic peak (P_2) caused by the reflected wave from small arteries; (iii) dicrotic (D) or the dicrotic peak (P_3) as a result of reflective oscillatory waves produced by the pressure of the aorta when the aortic valve is closed. By analyzing the radial artery pulse waveform that we attained, physiological information can be drawn, such as systolic upstroke time (UT), reflected wave transit time (RWTT), and augmentation index (AIx), as shown in Figure S10 [49, 52].

The RAPS was also prepared by other P(VDF-TrFE) solutions dissolved in DMF and DMSO. All the samples were treated by the SA method to enhance crystallinity and a portion of the β-phase. The drying process was performed at 90°C for 2 hours due to high boiling points of DMF and DMSO. Body pulses measured at the wrists by the RAPS based on DMF and DMSO are shown in Figures S11 and S12. Regardless of the solvents, all of the RAPS demonstrated excellent conversion of subtle pressure of radial artery pulses into electrical ones. This suggests that our new method is effective to improve the piezoelectric output response of the

standalone P(VDF-TrFE) film and has a great potential as a self-powered nondestructive biosensor application for continuous real-time health monitoring. Performance comparison of piezoelectric biosensors for various health monitoring applications is provided in Table S1.

In addition, the RAPS exhibited excellent stability against repeated mechanical strains of over one million cycles (Figure 6(d)) to simulate inputs of radial artery pulses over a longer period of time. The mechanical input was applied by the linear motor at the input frequency of 100 Hz to facilitate the long-term stability test of the RAPS. Figure 6(e) illustrates the enlarged voltage-time curves in Figure 6(d) at the beginning, intermediate, and terminal stages of the stability test. There was no significant reduction in output response and distortion of curve shapes.

Lastly, we further evaluated the long-term stability of the RAPS when the device was exposed to sweat in real applications. Sweat includes various minerals and metabolites, such as sodium, potassium, chloride, and urea. Because the amount of these substances in sweat is generally small, for example, 70 mmol/L (Na^+) and 55 mmol/L (Cl^-), we used 10 g of NaCl in 100 mL of DI water (approx. 2 M NaCl solution) containing 28- and 36-times larger amounts of Na^+ and Cl^- than in sweat to accelerate aging of the device stability. The RAPS was kept inside of the 2 M NaCl solution for about a week, and it was found that the RAPS worked for more than 3 days as shown in Figure S13. By rough approximation, this gives us 108 days (3 days × 36) of device stability without any passivation. In fact, the device would generally be exposed to sweat for less than 24 hours per day; the actual device stability is expected to be longer than 108 days, which will be further extended through the passivation of the device in practice.

4. Conclusion

We introduced a unique method to prepare a transparent standalone P(VDF-TrFE) film. The standalone polymer film

is an essential requirement to build wearable or patchable biomedical devices as devices with other supporting layers has limited wearability or patchability due to the thickness. In addition, based on the new annealing method employed, called solvent vapor annealing, high crystalline P(VDF-TrFE) with a higher portion of the β-phase was attained. Specifically, DSC analysis revealed that the percentage crystallinity (X_C) increased from 19.56 to 23.13%, FTIR showed that the portion of the β-phase increased from 82.51 to 84.35%, and FHWM of the XRD peak was reduced from 0.77 to 0.69°. This provides a viable solution to resolve the weak piezoelectric output response of P(VDF-TrFE) which has limited the use of PVDF-based polymers for biomedical applications. This was further proven by the surface potential and PFM measurement where the voltage increased from 116.51 to 221.17 V and 22.55 pm/V to 25.46 pm/V, respectively. Due to the enhanced piezoelectric output response, the biosensor based on PENG was able to detect subtle pressures in the range of 70–140 mmHg from radial artery pulses, generating the piezoelectric potential ranging from 14 to ~28 mV. Combining these two advantages, we achieved a transparent piezoelectric biosensor with a simple sandwiched structure, i.e., PENG, free from complex patterns or fabrication processes and toxic substances. Finally, our method provides a facile way to produce the P(VDF-TrFE) film with a high piezoelectric output performance without the conventional complex manufacturing processes, providing great practical values for future biomedical sensors.

Data Availability

Data are available on request.

Conflicts of Interest

There are no conflicts to declare.

Authors' Contributions

Yian Hu, Shunyao Huang, and Yujia Gao contributed equally to this work. Y.H., S.H., and Y.G. performed the data curation, formal analysis, investigation, and methodology. J.L. performed the formal analysis and visualization. Z.J. performed the data curation and formal analysis. G.-H.A. and Y.C. performed the validation, conceptualization, funding acquisition, supervision, and writing.

Acknowledgments

Supplementary Materials

Figure S1: FTIR measurement of SA-TrFE and TA-TrFE. Figure S2: thicknesses of SA-TrFE and TA-TrFE films measured using Dektak. Figure S3: transmittance of the adhesive conductive electrode on a glass substrate. Figure S4: surface potential of P(VDF-TrFE) films. (a) As-coated; (b) thermal annealing (TA); (c) solvent vapor annealing and dried (SA). Figure S5: I-V characteristics of the piezoelectric biosensor and its impedance. Figure S6: PFM amplitude and phase images of SA-TrFE and TA-TrFE film. Figure S7: characterization of piezoelectric response under relatively low frequencies by fabricating piezoelectric nanogenerators. (a) 3, (b) 5, (c) 10, (d) 20, (e) 30, and (f) 40 Hz. Figure S8: characterization of piezoelectric response under relatively high frequencies by fabricating piezoelectric nanogenerators. (a) 60, (b) 90, (c) 120, and (d) 150 Hz. Figure S5: output responses of RAPS based on MEK by measuring radial artery pulses of three volunteers. Figure S9: output response of RAPS based on MEK by measuring radial artery pulses of three volunteers. Figure S10: various physiological information which can be attained by the output response. Figure S11: output responses of RAPS based on DMF by measuring radial artery pulses of three volunteers. Figure S12: output responses of RAPS based on DMSO by measuring radial artery pulses of three volunteers. Figure S13: the long-term stability of the piezoelectric biosensor in the 2 M NaCl solution for the accelerated aging test. Table S1: performance comparison of piezoelectric biosensors for various applications. (*Supplementary Materials*)

References

[1] C. Mikton, V. de la Fuente-Núñez, A. Officer, and E. Krug, "Ageism: a social determinant of health that has come of age," *Lancet*, vol. 397, no. 10282, pp. 1333-1334, 2021.

[2] S. H. Kwon and L. Dong, "Flexible sensors and machine learning for heart monitoring," *Nano Energy*, vol. 102, p. 107632, 2022.

[3] Y. Fang, Y. Zou, J. Xu et al., "Ambulatory cardiovascular monitoring via a machine-learning-assisted textile triboelectric sensor," *Advanced Materials*, vol. 33, no. 41, p. e2104178, 2021.

[4] P. Tan, Y. Xi, S. Chao et al., "An artificial intelligence-enhanced blood pressure monitor wristband based on piezoelectric nanogenerator," *Biosensors*, vol. 12, no. 4, p. 234, 2022.

[5] X. Cao, Y. Xiong, J. Sun, X. Zhu, Q. Sun, and Z. L. Wang, "Piezoelectric nanogenerators derived self-powered sensors for multifunctional applications and artificial intelligence," *Advanced Functional Materials*, vol. 31, no. 33, article 2102983, 2021.

[6] X. Huang, Q. Qin, X. Wang et al., "Piezoelectric nanogenerator for highly sensitive and synchronous multi-stimuli sensing," *ACS Nano*, vol. 15, no. 12, pp. 19783–19792, 2021.

[7] H. Ouyang, D. Jiang, Y. Fan, Z. Wang, and Z. Li, "Self-powered technology for next-generation biosensor," *Scientific Bulletin*, vol. 66, pp. 1709–1712, 2021.

[8] J. Wang, Y. Zhu, Z. Wu et al., "Wearable multichannel pulse condition monitoring system based on flexible pressure sensor arrays," *Microsystems & Nanoengineering*, vol. 8, no. 1, p. 16, 2022.

[9] X. Chen, Y. Song, Z. Su et al., "Flexible fiber-based hybrid nanogenerator for biomechanical energy harvesting and physiological monitoring," *Nano Energy*, vol. 38, pp. 43–50, 2017.

[10] S. Bhunia, S. Chandel, S. K. Karan et al., "Autonomous self-repair in piezoelectric molecular crystals," *Science*, vol. 373, no. 6552, pp. 321–327, 2021.

[11] S. Yoon, J. K. Sim, and Y.-H. Cho, "A flexible and wearable human stress monitoring patch," *Scientific Reports*, vol. 6, no. 1, p. 23468, 2016.

[12] S. K. Karan, S. Maiti, A. K. Agrawal et al., "Designing high energy conversion efficient bio-inspired vitamin assisted single-structured based self-powered piezoelectric/wind/acoustic multi-energy harvester with remarkable power density," *Nano Energy*, vol. 59, pp. 169–183, 2019.

[13] S. Ojha, S. Paria, S. K. Karan et al., "Morphological interference of two different cobalt oxides derived from a hydrothermal protocol and a single two-dimensional metal organic framework precursor to stabilize the β-phase of PVDF for flexible piezoelectric nanogenerators," *Nanoscale*, vol. 11, no. 47, pp. 22989–22999, 2019.

[14] S. Huang, Y. Gao, Y. Hu, F. Shen, Z. Jin, and Y. Cho, "Recent development of piezoelectric biosensors for physiological signal detection and machine learning assisted cardiovascular disease diagnosis," *RSC Advances*, vol. 13, no. 42, pp. 29174–29194, 2023.

[15] Y. Chu, J. Zhong, H. Liu et al., "Human pulse diagnosis for medical assessments using a wearable piezoelectret sensing system," *Advanced Functional Materials*, vol. 28, no. 40, article 1803413, 2018.

[16] C. Dagdeviren, Y. Su, P. Joe et al., "Conformable amplified lead zirconate titanate sensors with enhanced piezoelectric response for cutaneous pressure monitoring," *Nature Communications*, vol. 5, no. 1, p. 4496, 2014.

[17] N. Wu, X. Cheng, Q. Zhong et al., "Cellular polypropylene piezoelectret for human body energy harvesting and health monitoring," *Advanced Functional Materials*, vol. 25, no. 30, pp. 4788–4794, 2015.

[18] D. Y. Park, D. J. Joe, D. H. Kim et al., "Self-powered real-time arterial pulse monitoring using ultrathin epidermal piezoelectric sensors," *Advanced Materials*, vol. 29, no. 37, article 1702308, 2017.

[19] Q. Zhang, T. Jiang, D. Ho et al., "Transparent and self-powered multistage sensation matrix for mechanosensation application," *ACS Nano*, vol. 12, no. 1, pp. 254–262, 2018.

[20] C. Wang, Y. Hu, Y. Shan et al., "Tissue-adhesive piezoelectric soft sensor for in vivo blood pressure monitoring during surgical operation," *Advanced Functional Materials*, vol. 33, no. 38, 2023.

[21] S. Min, D. H. Kim, D. J. Joe et al., "Clinical validation of a wearable piezoelectric blood-pressure sensor for continuous health monitoring," *Advanced Materials*, vol. 35, no. 26, article 2301627, 2023.

[22] R. Sun, S. C. Carreira, Y. Chen et al., "Stretchable piezoelectric sensing systems for self-powered and wireless health monitoring," *Advanced Materials Technologies*, vol. 4, no. 5, article 1900100, 2019.

[23] L. Persano, C. Dagdeviren, Y. Su et al., "High performance piezoelectric devices based on aligned arrays of nanofibers of poly(vinylidenefluoride-co-trifluoroethylene)," *Nature Communications*, vol. 4, no. 1, p. 1633, 2013.

[24] X. Pu, H. Guo, Q. Tang et al., "Rotation sensing and gesture control of a robot joint via triboelectric quantization sensor," *Nano Energy*, vol. 54, pp. 453–460, 2018.

[25] H. Guo, X. Pu, J. Chen et al., "A highly sensitive, self-powered triboelectric auditory sensor for social robotics and hearing aids," *Science Robotics*, vol. 3, no. 20, article eaat2516, 2018.

[26] X.-Z. Chen, J.-H. Liu, M. Dong et al., "Magnetically driven piezoelectric soft microswimmers for neuron-like cell delivery and neuronal differentiation," *Materials Horizons*, vol. 6, no. 7, pp. 1512–1516, 2019.

[27] J. Yang, Q. Chen, F. Xu et al., "Epitaxy enhancement of piezoelectric properties in P(VDF-TrFE) copolymer films and applications in sensing and energy harvesting," *Advanced Electronic Materials*, vol. 6, no. 10, article 2000578, 2020.

[28] D. Xu, H. Zhang, Y. Wang et al., "Piezoelectric biomaterials for neural tissue engineering," *Smart Medicine*, vol. 2, no. 2, article e20230002, 2023.

[29] S. C. Park, C. Nam, C. Baek, M.-K. Lee, G.-J. Lee, and K.-I. Park, "Enhanced piezoelectric performance of composite fibers based on lead-free BCTZ ceramics and P(VDF-TrFE) piezopolymer for self-powered wearable sensors," *ACS Sustainble*, vol. 10, no. 43, pp. 14370–14380, 2022.

[30] Y.-K. Fuh, P.-C. Chen, Z.-M. Huang, and H.-C. Ho, "Self-powered sensing elements based on direct-write, highly flexible piezoelectric polymeric nano/microfibers," *Nano Energy*, vol. 11, pp. 671–677, 2015.

[31] Z. Lou, S. Chen, L. Wang, K. Jiang, and G. Shen, "An ultrasensitive and rapid response speed graphene pressure sensors for electronic skin and health monitoring," *Nano Energy*, vol. 23, pp. 7–14, 2016.

[32] S.-H. Park, H. B. Lee, S. M. Yeon, J. Park, and N. K. Lee, "Flexible and stretchable piezoelectric sensor with thickness-tunable configuration of electrospun nanofiber mat and elastomeric substrates," *ACS Applied Materials & Interfaces*, vol. 8, no. 37, pp. 24773–24781, 2016.

[33] D. De Fazio, D. G. Purdie, A. K. Ott et al., "High-mobility, wet-transferred graphene grown by chemical vapor deposition," *ACS Nano*, vol. 13, no. 8, pp. 8926–8935, 2019.

[34] T. Nishiyama, T. Sumihara, E. Sato, and H. Horibe, "Effect of solvents on the crystal formation of poly(vinylidene fluoride) film prepared by a spin-coating process," *Polymer Journal*, vol. 49, no. 3, pp. 319–325, 2017.

[35] S. Maji, P. K. Sarkar, L. Aggarwal et al., "Self-oriented β-crystalline phase in the polyvinylidene fluoride ferroelectric and piezo-sensitive ultrathin Langmuir–Schaefer film," *Physical Chemistry Chemical Physics*, vol. 17, no. 12, pp. 8159–8165, 2015.

[36] Y. Cho, J. B. Park, B.-S. Kim et al., "Enhanced energy harvesting based on surface morphology engineering of P(VDF-TrFE) film," *Nano Energy*, vol. 16, pp. 524–532, 2015.

[37] Y. Cho, D. Ahn, J. B. Park et al., "Enhanced ferroelectric property of P(VDF-TrFE-CTFE) film using room-temperature crystallization for high-performance ferroelectric device applications," *Advanced Electronic Materials*, vol. 2, no. 10, article 1600225, 2016.

[38] J. Kim, J. H. Lee, H. Ryu et al., "High-performance piezoelectric, pyroelectric, and triboelectric nanogenerators based on P(VDF-TrFE) with controlled crystallinity and dipole alignment," *Advanced Functional Materials*, vol. 27, no. 22, article 1700702, 2017.

[39] Z. Fang, K. H. Chan, X. Lu, C. F. Tan, and G. W. Ho, "Surface texturing and dielectric property tuning toward boosting of triboelectric nanogenerator performance," *Journal of Materials Chemistry A*, vol. 6, no. 1, pp. 52–57, 2018.

[40] K. Y. Lee, S. K. Kim, J.-H. Lee et al., "Controllable charge transfer by ferroelectric polarization mediated triboelectricity," *Advanced Functional Materials*, vol. 26, no. 18, pp. 3067–3073, 2016.

[41] R. Gregorio Jr. and M. M. Botta, "Effect of crystallization temperature on the phase transitions of P(VDF/TrFE) copolymers," *Journal of Polymer Science Part B: Polymer Physics*, vol. 36, no. 3, pp. 403–414, 1998.

[42] Y. Li, W. Feng, L. Meng et al., "Investigation on in-situ sprayed, annealed and corona poled PVDF-TrFE coatings for guided wave-based structural health monitoring: from crystallization to piezoelectricity," *Materials & Design*, vol. 199, article 109415, 2021.

[43] A. Lonjon, L. Laffont, P. Demont, E. Dantras, and C. Lacabanne, "Structural and electrical properties of gold nanowires/P(VDF-TrFE) nanocomposites," *Journal of Physics D*, vol. 43, no. 34, article 345401, 2010.

[44] J. Choi, K. Lee, M. Lee et al., "High β-phase poly(vinylidene fluoride) using a thermally decomposable molecular splint," *Advanced Electronic Materials*, vol. 9, no. 1, article 2200279, 2023.

[45] X. Cai, T. Lei, D. Sun, and L. Lin, "A critical analysis of the α, β and γ phases in poly(vinylidene fluoride) using FTIR," *RSC Advances*, vol. 7, no. 25, pp. 15382–15389, 2017.

[46] N. Turdakyn, Z. Bekezhankyzy, S. Araby, R. Montazami, Z. Bakenov, and G. Kalimuldina, "Investigation of electrospun piezoelectric P(VDF-TrFE) nanofiber-based nanogenerators for energy harvesting," *Energy Reports*, vol. 10, pp. 628–636, 2023.

[47] Z. Yi, Z. Liu, W. Li et al., "Piezoelectric dynamics of arterial pulse for wearable continuous blood pressure monitoring," *Advanced Materials*, vol. 34, no. 16, article e2110291, 2022.

[48] A. Petritz, E. Karner-Petritz, T. Uemura et al., "Imperceptible energy harvesting device and biomedical sensor based on ultraflexible ferroelectric transducers and organic diodes," *Nature Communications*, vol. 12, no. 1, p. 2399, 2021.

[49] J. Chen, H. Liu, W. Wang et al., "High durable, biocompatible, and flexible piezoelectric pulse sensor using single-crystalline III-N thin film," *Advanced Functional Materials*, vol. 29, no. 37, article 1903162, 2019.

[50] Z. Yi, J. Huang, Z. Liu, J. Liu, and B. Yang, "Portable, wireless wearable piezoelectric arterial pulse monitoring system based on near-field communication approach," *IEEE Electron Device Letters*, vol. 2020, pp. 183–186, 2019.

[51] G. D'ambrogio, O. Zahhaf, M. Bordet et al., "Structuring BaTiO$_3$/PDMS nanocomposite via dielectrophoresis for fractional flow reserve measurement," *Advanced Engineering Materials*, vol. 23, no. 10, article 2100341, 2021.

[52] K. Kohara, Y. Tabara, A. Oshiumi, Y. Miyawaki, T. Kobayashi, and T. Miki, "Radial augmentation index: a useful and easily obtainable parameter for vascular aging," *American Journal of Hypertension*, vol. 18, 1 Part 2, pp. 11S–14S, 2005.

[53] Y. Cho, P. Giraud, B. Hou et al., "Charge transport modulation of a flexible quantum dot solar cell using a piezoelectric effect," *Advanced Energy Materials*, vol. 8, no. 3, article 1700809, 2018.

[54] Y. Cho, B. Hou, P. Giraud, S. Pak, and S. Cha, "Ferroelectric field effect induced charge carrier transport modulation at quantum dot solar cell heterojunction Interface," *ACS Applied Energy Materials*, vol. 4, no. 11, pp. 12056–12062, 2021.